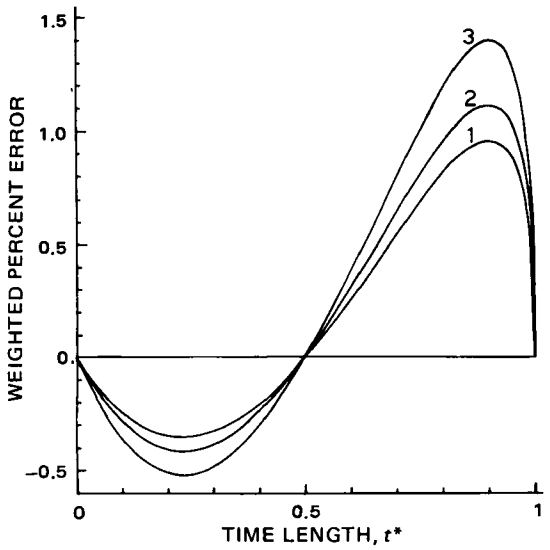

Figure 7—*Graph of errors in the spherical approximation (Eq. 32) to the dissolution (Eq. 25) of a monoclinic or rhombic prismatic particle of different shape ratios. The error is weighted proportionally to the fraction undissolved* (w/w_0). *Key: 1,* $F_2 = 1/8$; *2,* $F_2 = 1/4$; *and 3,* $F_2 = 1/3$. $F_1 = 1/2$.

The basic assumption behind these derivations is that the rate of dissolution per unit surface area, J, remains constant during dissolution and is the same everywhere at the interface of the dissolving crystal. This assumption can only be approximately true in practice under complete sink conditions. The higher activity at the crystal edges results in a larger J value in these areas and, therefore, a "rounding off" of the shape, so that dissolution in the later stages is slower than that calculated. However, this should result in an *improvement* in the fit of the spherical approximation and sometimes may result in a closer fit to the real dissolution than the exact expressions given for isotropic conditions. Thus, the approximating curve (stippled line, Figs. 4 and 6) is above the calculated dissolution curve in the later stages. The *true* dissolution curve, because of the rounding off effect, is above the calculated curve and hence closer to the approximation.

Excellent agreement between experimental and calculated results was obtained for the dissolution of a multiparticulate system of particles, approximately tetragonal prismatic in shape, when the respective spherical approximations were applied (9).

REFERENCES

(1) J. P. Cleave, *J. Pharm. Pharmacol.*, **17**, 698(1965).

(2) J. Cobby, M. Mayersohn, and G. C. Walker, *J. Pharm. Sci.*, **63**, 725(1974).

(3) I. C. Edmundson and K. A. Lees, *J. Pharm. Pharmacol.*, **17**, 193(1965).

(4) R. J. Withey, *ibid.*, **23**, 573(1971).

(5) A. W. Hixson and J. H. Crowell, *Ind. Eng. Chem.*, **23**, 923(1931).

(6) P. Veng Pedersen and K. F. Brown, *J. Pharm. Sci.*, **64**, 1981(1975).

(7) P. J. Niebergall, G. Milosovich, and J. E. Goyan, *ibid.*, **52**, 236(1963).

(8) P. Veng Pedersen and K. F. Brown, *ibid.*, **64**, 1192(1975).

(9) *Ibid.*, **65**, 1442(1976).

ACKNOWLEDGMENTS AND ADDRESSES

Received May 2, 1975, from the *Department of Pharmacy, University of Sydney, Sydney, N.S.W. 2006, Australia.*

Accepted for publication December 10, 1975.

Supported in part by Grant 72.4244 from the National Health and Medical Research Council of Australia.

[x] To whom inquiries should be directed.

Experimental Evaluation of Three Single-Particle Dissolution Models

PETER VENG PEDERSEN [x] and K. F. BROWN

Abstract □ The dissolution of the 60–85-mesh fraction of tolbutamide was investigated using a high precision, continuous recording, flow-through dissolution apparatus equipped with a dissolution cell; it was particularly suitable for kinetic analysis of multiparticulate systems. By using a time-scaling approach, experimental data are compared with theoretical calculations to evaluate, quantitatively, which of three single-particle dissolution models best describes the data and how well the multiparticulate kinetics can be explained mathematically. The nonspherical tolbutamide particles are replaced in the calculations by a hypothetical system of spherical particles that appears to be log-normally distributed. This procedure permits the calculation of the intrinsic dissolution profile, considering both size distribution and particle shape effects.

Keyphrases □ Dissolution—tolbutamide, three single-particle models evaluated and compared, mathematical analysis □ Tolbutamide—dissolution, three single-particle models evaluated and compared, mathematical analysis

There are several kinetic models for single-particle dissolution. Experimental evaluation of these models has been based on multiparticulate dissolution data, but distribution and particle shape effects have not been considered. The general theory of multiparticulate dissolution was discussed previously (1). This theory was subsequently used to develop mathematical expressions for the dissolution of log-normally distributed powders, considering three single-particle dissolution models (2).

A recent publication (3) dealt with the theory of single-particle dissolution in relation to particle shape. It gives directions for calculating the diameter of hypothetical spherical particles whose dissolution approximates nonspherical particles with minimum error. This paper demonstrates the application of

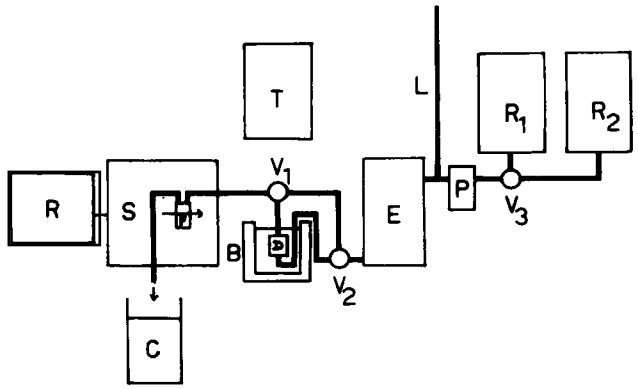

Figure 1—*Diagram of continuous-flow recording dissolution apparatus. (See text for description.)*

these theories to explain the dissolution kinetics of the 60–85-mesh fraction of tolbutamide such that both size distribution effects (2) and particle shape effects (3) are considered. By using a time-scaling approach, the three single-particle dissolution kinetic models are evaluated.

EXPERIMENTAL

A continuous-flow recording dissolution apparatus was used (Fig. 1). As shown in Fig. 1, R_1 and R_2 are 20-liter reservoirs containing the dissolution liquid, and P is a pulse-free peristaltic pump transporting liquid from R_1 or R_2 through a heat exchanger, E, which adjusts the liquid to the required temperature before it reaches the dissolution cell, D. This cell is immersed in a water-filled, jacketed beaker, B, maintained at the same temperature as the dissolution liquid leaving E. Liquid from dissolution cell D passes through a flowcell, F, in the spectrophotometer, S, fitted with a chart recorder, R, and finally accumulates in the collection vessel, C.

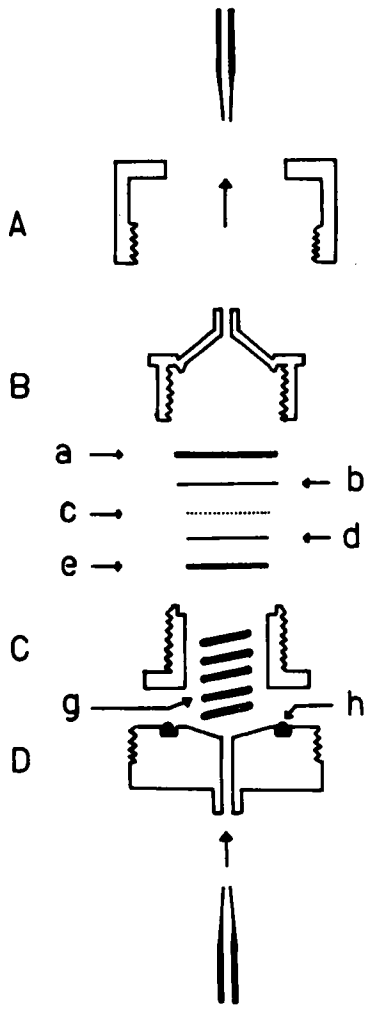

Figure 2—*Enlarged diagram of dissolution cells. (See text for description.)*

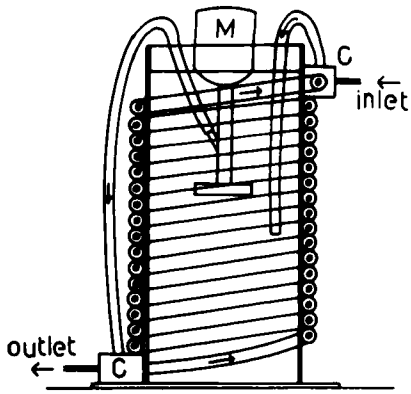

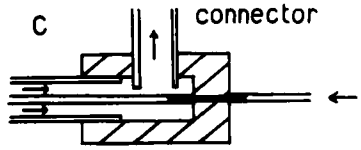

Figure 3—*Diagram of heat exchanger. (See text for description.)*

Two-way valves, V_1 and V_2, enable bypass of dissolution cell D for zero-line adjustment of the spectrophotometer with blank liquid from the reservoir; V_3 is a similar valve through which liquid can be drawn from either reservoir R_1 or R_2. Polyethylene tubing (i.d. 0.35 cm) was used throughout. The pressure governing the flow rate is monitored by the open tube-type meter L.

Figure 2 shows a detailed diagram of the dissolution cell constructed for this work. Powder to be investigated is spread in a single particle layer, c, in a sandwich line arrangement between two paper filters, b and d[1]. These filters are supported on both sides by stainless steel filter supports, a and e[2]. Filter support e and filter d have a diameter equal to the inside diameter of C (2.20 cm), whereas a and b have the same diameter as the recess in C; B and C are modified portions of a 2.54-cm (1-in.) filter holder unit[3].

Part C was modified from the commercial filter unit by increasing the depth of the recess to contain both a and b. In addition, a hole 2.20 cm in diameter was bored through the center. A watertight pressure seal is achieved by means of an O-ring, h.

The equipment for temperature regulation was also designed especially for this work to overcome the problems of maintaining large volumes of dissolution fluid at a constant temperature (Fig. 3). It consists of a cylindrical polyvinyl chloride reservoir, 40 cm in depth with internal diameter 15.5 cm, filled with distilled water. A thermostat water circulator, M, is mounted in this cylinder and connected to a polyvinyl chloride hose, which is coiled around the outer surface of the cylinder. Heated water from the cylinder is continuously recycled through the hose and returned to the reservoir. Polyethylene tubing is threaded inside the hose, carrying the dissolution fluid which requires temperature regulation.

Dissolution fluid is transported *via* the peristaltic pump and flows countercurrent to the recycled water through the inner polyethylene hose. Stainless steel connectors, C, seal the polyvinyl chloride hose at the points of entry and exit of the small bore tubing. This apparatus is very efficient in providing dissolution liquid at a constant temperature. When the water in the reservoir is

[1] Whatman quantitative filter paper.
[2] Millipore Catalog No. xx 3002503.
[3] Gelman.

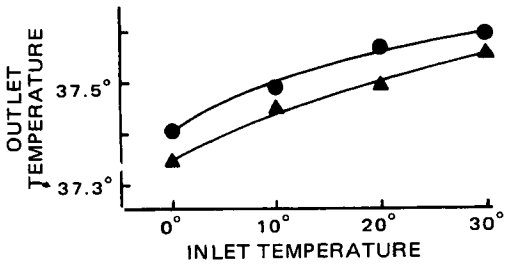

Figure 4—*Variation in temperature of water, after passage through heat exchanger, as a function of inlet water temperature. Thermostat setting was 37.7°. Key: ●, 0.24-ml/sec flow rate; and ▲, 1.90-ml/sec flow rate.*

maintained at 37.7°, the temperature of the dissolution liquid leaving the heat exchanger is 37.5 ± 0.2° for inlet temperatures ranging between 0 and 30° and flow rates of 0.24–1.90 ml/sec (Fig. 4).

Values of absorbance were read from the chart recording at 1–2.5-min intervals from the beginning of the experiment. These data, together with the volumetric flow rate, the Beer law constant, the initial amount of drug used, and the amount undissolved remaining in the dissolution cell at the end of the experiment, were processed by digital computer according to a FORTRAN program. This procedure permitted the evaluation of various dissolution kinetic models. Hydrochloric acid, 0.1 *M*, was used as liquid for all dissolution tests.

The accuracy of the apparatus in combination with the computer treatment was tested using 12.5 mg of the 60–85-mesh fraction of tolbutamide and a flow rate of 0.568 ml/sec (0.149 cm/sec linear flow rate). Dissolution liquid containing dissolved drug was collected at intervals of exactly 5 min as it left the spectrophotometer flowcell (F, Fig. 1) and was assayed for drug. Cube root plots (Fig. 5) of the dissolution data obtained from direct analysis of the samples and plots generated by the computer from the spectrophotometer recording almost coincided. The difference was similar in magnitude to the observed variation in flow rate, which was less than 1%.

THEORY

The three equations (from Refs. 4–6, respectively) for dissolution of a spherical particle under sink conditions are:

$$w^{1/3} = w_0^{1/3} - k_1 t \qquad \text{(Eq. 1)}$$

$$w^{1/2} = w_0^{1/2} - k_2 t \qquad \text{(Eq. 2)}$$

$$w^{2/3} = w_0^{2/3} - k_3 t \qquad \text{(Eq. 3)}$$

or, in general form:

$$w = (w_0^{1/m} - kt)^m \qquad \text{(Eq. 4)}$$

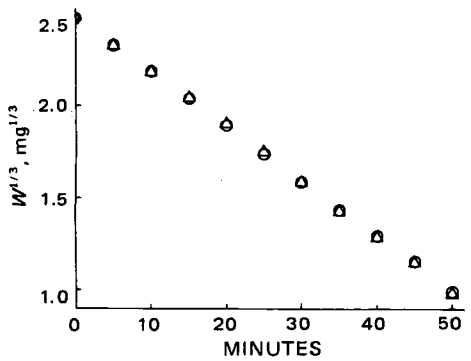

Figure 5—*Test of the accuracy of the dissolution apparatus in combination with the computer data treatment of the continuous chart recording. Dissolution is of 12.5 mg of the 60–85-mesh fraction of tolbutamide in 0.1 M HCl using dissolution cell at solvent flow rate of 0.149 cm/sec (0.568 ml/sec). Key: △, values calculated from intermittent samples collected at 5-min intervals; and ○, values generated by digital computer from continuous chart recording.*

where w and w_0 are the respective weights of the undissolved particle at times t and $t = 0$; $m = 3$, 2, and 3/2; and $k = k_1$, k_2, and k_3. The positive constants k_1, k_2, and k_3 replace the original coefficients of time. These contain quantities such as density, the diffusion coefficient, and the shape factor that are considered constant. This simplification is made because the aim is not to evaluate the theoretical basis of the three equations but solely to assess them as models for describing the dissolution kinetic data. They will be denoted as the "cube root," the "square root," and the "squared cube root" models for Eqs. 1, 2, and 3, respectively, corresponding to $m = 3$, 2, and 3/2 in Eq. 4.

These equations do not strictly describe the dissolution correctly in their present form since w does not vanish for $t \to \infty$. A more correct formulation would be:

$$w = (w_0^{1/m} - kt)^n \quad \text{for} \quad t < w_0^{1/m}/k \qquad \text{(Eq. 5a)}$$

$$w = 0 \quad \text{for} \quad t \geq w_0^{1/m}/k \qquad \text{(Eq. 5b)}$$

The general multiparticulate dissolution equation presented earlier (Eq. 13, Ref. 1), however, accepts the single-particle dissolution function in the forms of both Eqs. 4 and 5. Equation 4 will be used for simplicity.

In a previous paper (2), the following equations were presented to describe the dissolution profile of a multiparticulate system where the spherical particles dissolve according to each of the three models:

$$\frac{W}{W_0} = \sum_{n=0}^{m} \binom{m}{n} (-Kt)^{(m-n)} \times \frac{F\left(\frac{T_2 - \mu}{\sigma} - \frac{3n\sigma}{m}\right) - F\left(\frac{T_1 - \mu}{\sigma} - \frac{3n\sigma}{m}\right)}{F(j - 3\sigma) - F(-i - 3\sigma)} e^{\frac{3}{m}(n-m)\left[\mu + \frac{3}{m}(n+m)\frac{\sigma^2}{2}\right]} \qquad \text{(Eq. 6)}$$

where $m = 3$ (Eq. 6a) and $m = 2$ (Eq. 6b) and:

$$T_1 = \mu - i\sigma \quad \text{for} \quad \frac{m}{3} \ln (Kt) < \mu - i\sigma$$

$$T_1 = \frac{m}{3} \ln (Kt) \quad \text{for} \quad \frac{m}{3} \ln (Kt) \geq \mu - i\sigma$$

$$T_2 = \mu + j\sigma \quad \text{for} \quad \frac{m}{3} \ln (Kt) < \mu + j\sigma$$

$$T_2 = \frac{m}{3} \ln (Kt) \quad \text{for} \quad \frac{m}{3} \ln (Kt) \geq \mu + j\sigma$$

$$\binom{m}{n} = \frac{m!}{(m-n)!n!}$$

Furthermore ($m = 3/2$):

$$\frac{W}{W_0} = \frac{\int_{R_1}^{R_2} (w^2 - Kt)^{3/2} w^{-1} N(\ln w, \mu, \sigma) dw}{F(j - 3\sigma) - F(-i - 3\sigma)} e^{-3\mu - 9\sigma^2/2} \qquad \text{(Eq. 6c)}$$

where:

$$R_1 = e^{\mu - i\sigma} \quad \text{for} \quad (Kt)^{1/2} < e^{\mu - i\sigma}$$

$$R_1 = (Kt)^{1/2} \quad \text{for} \quad (Kt)^{1/2} \geq e^{\mu - i\sigma}$$

$$R_2 = e^{\mu + j\sigma} \quad \text{for} \quad (Kt)^{1/2} < e^{\mu + j\sigma}$$

$$R_2 = (Kt)^{1/2} \quad \text{for} \quad (Kt)^{1/2} \geq e^{\mu + j\sigma}$$

The function $F(\ )$ is the area under the standard normal curve function defined by:

$$F(x) = \int_{-\infty}^{x} (1/\sqrt{2\pi}) e^{-\frac{x^2}{2}} dx \qquad \text{(Eq. 7)}$$

The function $N(\ln w, \mu, \sigma)$ is the normal distribution function with the natural logarithm to w as the variable, defined by:

$$N(\ln w, \mu, \sigma) = \frac{1}{\sigma\sqrt{2\pi}} e^{-1/2\left(\frac{\ln w - \mu}{\sigma}\right)^2} \qquad \text{(Eq. 8)}$$

The constant K is related to k_1, k_2, and k_3 (Eqs. 1–3) by:

$$K = (6/\rho\pi)^{1/m} k_i \qquad \text{(Eq. 9)}$$

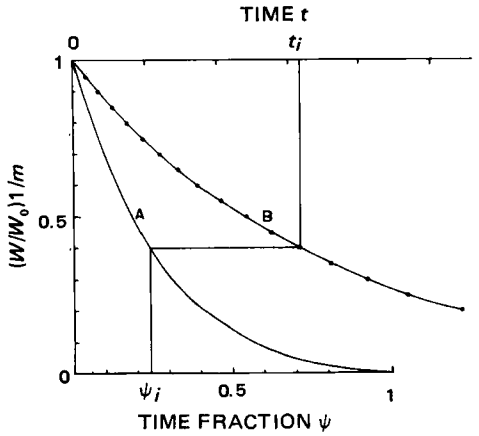

Figure 6—*Time-scaling approach (Eqs. 11–14) used in Figs. 8–10 to evaluate the agreement between the observed dissolution data (●) and the theoretical dissolution curve calculated in the form of the normalized intrinsic dissolution profile (A) on the basis of particle-size analysis.*

where ρ is the particle density, and $i = 1, 2, 3$. It is assumed that the particle diameter (a) distribution is "log normal"; that is, ln a can be approximated by a normal distribution (mean = μ, standard deviation = σ) truncated at the lower end at $\mu - i\sigma$ and at the upper end at $\mu + j\sigma$, where i and j are truncation parameters.

The multiparticulate dissolution equations (Eqs. 6*a*–6*c*) consider spherical drug particles. Such particles are only encountered when the drug exists in liquid form as an emulsion. In solid form, the particles are not spherical. The drug used for the dissolution tests was a 60–85-mesh fraction of tolbutamide consisting of particles approximately tetragonal prismatic in shape. A previous theoretical paper (3) showed that the dissolution of such particles could be approximated well by the dissolution of hypothetical spherical particles. The equivalent spherical diameter, a, is the diameter of the spherical particle that best approximates the dissolution of the nonspherical particle and is given by:

$$a = \frac{b_0}{2 - \left(2 - \frac{b_0}{l_0}\right)^{1/3}} \qquad \text{(Eq. 10)}$$

where l_0 and b_0 are the length and side, respectively, of the tetragonal particle. In this way, dissolution of the nonspherical particle system can be suitably described by the dissolution of a hypothetical spherical particle system that can be rigorously treated using Eqs. 6*a*–6*c*.

It is evident that k, μ, σ, i, j, and ρ must be known to calculate the dissolution profile. The distribution parameters μ, σ, i, and j can be obtained from micrographs, and ρ can be obtained by a standard method; however, the single-particle rate parameter k is unknown. It is possible to calculate the exact intrinsic dissolution profile with much less information[4]. According to the rules given previously (2) for multiparticulate dissolution, only the *shape* of the initial distribution (*i.e.*, of these six parameters only σ, i, and j) is required to calculate the intrinsic dissolution profile when the single-particle dissolution model is known. The concept of time scaling also was discussed previously (2). By such an approach, it is possible to evaluate quantitatively the difference between the actual dissolution data and the calculated intrinsic dissolution profile.

Figure 6 illustrates this application of time scaling. Curve B, through the experimental data points, represents the dissolution curve [$(w/w_0)^{1/m}$ *versus* t]; curve A represents the corresponding calculated normalized intrinsic dissolution profile [$(w/w_0)^{1/m}$ *versus* ψ][4].

If N is the number of data points and f is the time-scaling factor that brings curve B "into" curve A, the sum of the squared deviations between the curves given by:

$$ss = \sum_{i=1}^{N}(ft_i - \psi_i)^2 \qquad \text{(Eq. 11)}$$

[4] The intrinsic dissolution profile and normalized intrinsic dissolution profile were defined and discussed previously (2).

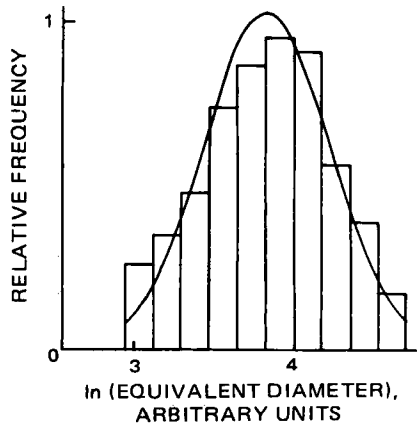

Figure 7—*Histogram of the logarithm of the equivalent spherical diameters of a sample of 500 particles from the 60–85-mesh fraction of tolbutamide powder used in the dissolution tests. The equivalent spherical diameters of the particles that are approximately tetragonal prismatic in shape were calculated according to Eq. 10 from measurements made (in arbitrary units) on electron micrographs. The parameters of the truncated log-normal distribution which best fit this diameter distribution are: σ = 0.395, μ = 3.82, i = 2.25, and j = 2.20.*

is a minimum when $\partial ss/\partial f = 0$, which gives:

$$f = \frac{\sum_{i=1}^{N}\psi_i t_i}{\sum_{i=1}^{N}t_i^2} \qquad \text{(Eq. 12)}$$

The minimum of the sum of squares is therefore:

$$ss = \sum_{i=1}^{N}\left[\left(\frac{\sum_{i=1}^{N}\psi_i t_i}{\sum_{i=1}^{N}t_i^2}\right)t_i - \psi_i\right]^2 \qquad \text{(Eq. 13)}$$

which can be simplified such that the mean squared deviation is given by:

$$\overline{ss} = \frac{1}{N}\sum_{i=1}^{N}\psi_i^2 - \frac{\left(\sum_{i=1}^{N}\psi_i t_i\right)^2}{N\sum_{i=1}^{N}t_i^2} \qquad \text{(Eq. 14)}$$

This expression is chosen as the basis for a quantitative judgment of how well the kinetic models fit the data[5].

RESULTS AND DISCUSSION

The logarithmic distribution of the equivalent spherical diameters of the 60–85-mesh fraction of tolbutamide used for the dissolution test was obtained from direct measurements of 500 particles on a series of 30 × 30-cm electron micrographs. These measurements were made in arbitrary units, disregarding the magnification power, because the calculation of the intrinsic dissolution profile does not require information about the actual sizes of the particles but only the shape of their distribution (σ, i, and j for a log-normal powder).

Each particle was approximated by the tetragonal prismatic body which fitted best, and its equivalent spherical diameter was calculated using Eq. 10. The histogram of the logarithm of these diameters (Fig. 7) shows a good fit to a normal distribution with standard deviation σ = 0.395 and mean μ = 3.82. The truncation

[5] The alternative approach to bring curve A into curve B that has the character of a curve fitting to the data points would yield the same result in a comparison of the models. The time scaling of the *data* is used for the convenience of plotting and to better illustrate the predicted time for complete dissolution.

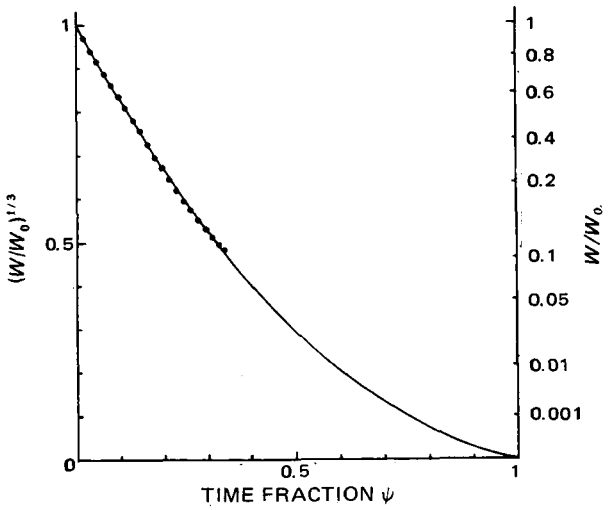

Figure 8—*Plot illustrating the agreement between data for the dissolution of 15 mg of tolbutamide (●) and the theoretical dissolution, considering the cube root model (Eq. 1) calculated (Eq. 6a) in the form of a normalized intrinsic dissolution profile using the parameters from the truncated log-normal distribution shown in Fig. 7. The data are time scaled using the scale factor given by Eq. 12. The mean squared deviation* $\overline{ss} = 1.10 \times 10^{-3}$.

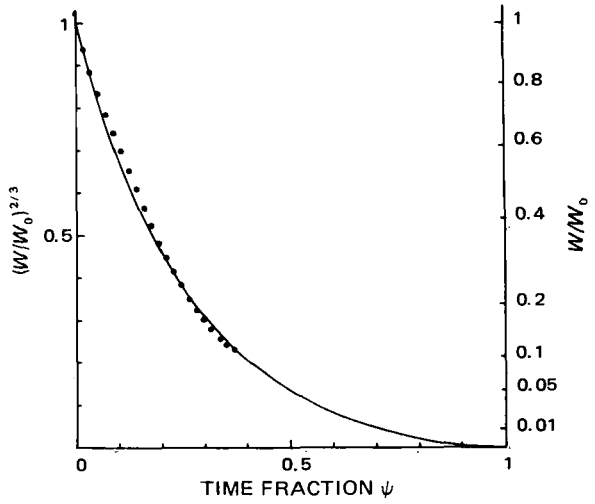

Figure 10—*Plot illustrating the agreement between data for the dissolution of 15 mg of tolbutamide (●) and the theoretical dissolution, considering the squared cube root model (Eq. 3), calculated (Eq. 6c) in the form of a normalized intrinsic dissolution profile using the parameters from the truncated log-normal distribution shown in Fig. 7. The data are time scaled using the scale factor given by Eq. 12. The mean squared deviation* $\overline{ss} = 6.70 \times 10^{-3}$.

parameters, $i = 2.25$ and $j = 2.20$, were obtained by dividing the distance from the mean to the end-points of the distribution by the standard deviation.

The normalized intrinsic dissolution profiles were calculated for each kinetic model, employing Eqs. 6a–6c and using the above values of the distribution shape parameters σ, i, and j (2). These calculated profiles are graphed as the continuous curves in Figs. 8–10, where the fraction of undissolved powder, W/W_0, is plotted according to the respective *single*-particle dissolution equation (Eqs. 1–3) to illustrate the nonlinearity caused by the distribution and particle shape effects. The same figures include a set of data for the dissolution of 15 mg of tolbutamide followed to about 90% dissolution[6]. These data are time scaled, using the optimal time-scaling factor given by Eq. 12, to illustrate the fit of the three models. The fit is very good for Eq. 6a, based on the cube root model ($\overline{ss} = 1.10 \times 10^{-3}$, Fig. 8) and for Eq. 6b, based on the square root model ($\overline{ss} = 1.92 \times 10^{-3}$, Fig. 9), but it is not so good for the squared cube root model ($\overline{ss} = 6.70 \times 10^{-3}$, Fig. 10).

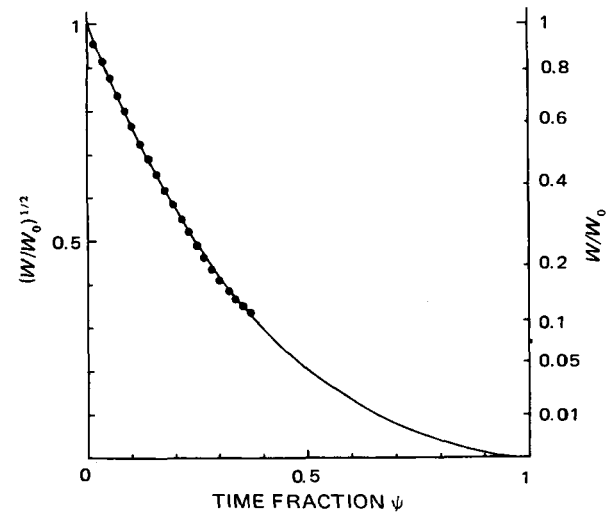

Figure 9—*Plot illustrating the agreement between data for the dissolution of 15 mg of tolbutamide (●) and the theoretical dissolution, considering the square root model (Eq. 2), calculated (Eq. 6b) in the form of a normalized intrinsic dissolution profile using the parameters from the truncated log-normal distribution shown in Fig. 7. The data are time scaled using the scale factor given by Eq. 12. The mean squared deviation* $\overline{ss} = 1.92 \times 10^{-3}$.

[6] The absorbance after 90% dissolution was so small that substantial error would have been introduced if the process had been followed much further.

The dissolution test was done several times using different amounts of tolbutamide. The $\overline{ss}$ values (Table I) indicate (F-test, $p < 0.05$) that the cube root model (Eq. 1) describes the single-particle dissolution best. The square root model (Eq. 2) is almost as good, but the squared cube root model is relatively poor.

To make the evaluations of the three models (Eqs. 1–3) by comparing dissolution data with theoretical calculations, it is necessary that the experimental conditions are consistent with the assumptions behind these calculations. A previous paper (2) discussed the three assumptions on which Eqs. 6a–6c are based:

1. The particles dissolve independently of each other. The apparatus constructed for this work is different from other published dissolution flowcell apparatus in that it guarantees this condition, which is of fundamental importance in the analysis of multiparticulate dissolution kinetics. This condition is achieved by the "absolute sink arrangement" of the drug particles in the dissolution cell. The particles are placed in a single layer such that in principle no particle receives solvent that has contacted other particles. The solvent thus contains no dissolved drug that may influence dissolution.

Table I—Mean Squared Deviation, $\overline{ss}$ (Eq. 14), as a Quantitative Comparison of the Fit of the Three Multiparticulate Dissolution Equations, Eqs. 6a–6c (Based on the Single-Particle Dissolution Models of Eqs. 1–3) to the Data from the Dissolution of Various Amounts of the 60–85-Mesh Fraction of Tolbutamide

Tolbutamide, mg	$\overline{ss} \times 10^3$		
	Eq. 6a	Eq. 6b	Eq. 6c
5	1.18	2.08	7.17
	1.22	2.20	7.40
	1.20	2.21	7.58
10	1.15	2.01	6.92
	1.21	2.18	7.41
	1.29	2.30	7.80
15	1.10	1.92	6.70
	1.19	2.10	7.12
	1.23	2.26	7.50
Mean	1.20	2.14	7.29
SE	0.050	0.119	0.337

2. The dissolution rate parameter [k_1, k_2, or k_3 (Eqs. 1–3)] is constant and the same for all particles. According to the theory on which the models are based, this condition can only be achieved experimentally if the temperature and composition of the dissolution liquid are maintained constant and the flow rate is constant or uniform in the cross section of the dissolution cell where the particles are placed.

The first two conditions are easily met. With regard to the flow rate, the dissolution cell used has a very useful feature: the process can be stopped and the cell rapidly disconnected, allowing the particles to be inspected at any stage of the dissolution process. Such inspections showed (after microscopic measurements) uniform dissolution over the whole particle layer, indicating a uniform flow rate. The fact that the particles in the dissolution cell can be inspected in this way makes it possible for dissolution data to be combined with particle-size measurements (2).

3. The initial particle-size (diameter) distribution can be approximated by a truncated log-normal distribution function. Figure 7 shows that this is the case for the 500 particles *measured*. However, it does not guarantee the correctness of the assumption that this small sample represents the particle-size distribution in the samples used for the dissolution tests, although optical investigations of the uniformity of the powder support this assumption.

This paper has shown that it is possible to describe mathematically the dissolution of a multiparticulate system with a high degree of accuracy by considering both the particle-size distribution effect and the particle shape effect discussed earlier (2, 3). It is evident from the dissolution data obtained that, of the three models investigated, the single-particle dissolution model (Eq. 1) describes the kinetics best.

More complex and flexible models for single-particle dissolution possibly could describe the dissolution more adequately. The fact that the *ss* values for the cube root and the square root model are almost the same suggests a model with properties between these two. The Danckwerts model, as discussed by Goyan (7), is given by:

$$-dw/dt = A[(Dp)^{1/2} + D/a]C_a \qquad \text{(Eq. 15)}$$

where w = weight undissolved, A = surface area, D = diffusion coefficient, p = quantity related to stirring, a = radius of the particle, and C_a = steady-state concentration.

This model is very flexible. When $(Dp)^{1/2}$ predominates, the apparent model would be the cube root model. As the quantity D/a becomes more important, the square root model becomes the apparent model. Finally, as the quantity D/a predominates, the squared cube root model becomes the apparent model. However, when applied to the log-normal case, the Danckwerts model results in a mathematical expression that is much more complex than Eqs. 6*a*–6*c*.

The fit of the dissolution data to the cube root model is excellent. Therefore, if an application of the Danckwerts model results in an even better fit, this improvement will most likely be statistically insignificant considering the magnitude of the experimental errors. The Hixon–Crowell model should be the preferred model in such a case because of its simplicity.

REFERENCES

(1) P. Veng Pedersen and K. F. Brown, *J. Pharm. Sci.*, **64,** 1192(1975).

(2) *Ibid.*, **64,** 1981(1975).

(3) *Ibid.*, **65,** 1437(1976).

(4) A. W. Hixson and J. H. Crowell, *Ind. Eng. Chem.*, **23,** 923(1931).

(5) P. J. Niebergall, G. Milosovich, and J. E. Goyan, *J. Pharm. Sci.*, **52,** 236(1963).

(6) W. I. Higuchi and E. N. Hiestand, *ibid.*, **52,** 67(1963).

(7) J. E. Goyan, *ibid.*, **54,** 645(1965).

ACKNOWLEDGMENTS AND ADDRESSES

Received May 2, 1975, from the *Department of Pharmacy, University of Sydney, Sydney, N.S.W. 2006, Australia.*

Accepted for publication July 1, 1975.

Supported in part by Grant 74/4244 from the National Health and Medical Research Council of Australia.

[x] To whom inquiries should be directed.

Antioxidant Efficiency of Polyhydric Phenols in Photooxidation of Benzaldehyde

DOUGLAS E. MOORE

Abstract □ An experimental system is described for the observation of the kinetics of photochemically initiated oxidation reactions; this system is based on the measurement of oxygen consumption with a polarographic oxygen electrode. The photooxidation of benzaldehyde in dilute aqueous solution was examined and appears to conform to a free radical chain mechanism. The antioxidant efficiency of some polyhydric phenols was determined kinetically and found to be catechol > pyrogallol > hydroquinone > resorcinol > *n*-propyl gallate for the benzaldehyde photooxidation.

Keyphrases □ Antioxidants—efficiency, various polyhydric phenols, photooxidation of benzaldehyde □ Phenols, polyhydric—antioxidant efficiency in photooxidation of benzaldehyde □ Photooxidation—benzaldehyde, antioxidant efficiency of various polyhydric phenols □ Benzaldehyde—photooxidation, antioxidant efficiency of various polyhydric phenols □ Oxidation, photochemical—benzaldehyde, antioxidant efficiency of various polyhydric phenols

The oxidative deterioration of pharmaceuticals can be initiated by UV light, both in the presence and absence of sensitizers. Two general classes of photooxidation reactions are recognized. The first is the free radical chain mechanism of autoxidation (1) initiated by sensitizers (such as benzophenone) that abstract a hydrogen atom from the oxidant. The free radical thus formed adds molecular oxygen and propagates the chain mechanism by abstracting hydrogen from a further oxidant molecule, giving rise to a hydroperoxide. The hydroperoxide is the major product but usually reacts further by a slower nonradical disproportionation mechanism. For example, it was shown (2) that the peroxy acid formed during aldehydic autoxidation undergoes an acid–base-catalyzed decomposition reaction to the carboxylic acid, which is the final reaction product.

The second class is the dye-sensitized (*e.g.*, methylene blue) photooxygenation of acceptors (3). These acceptors are either: (*a*) cyclic dienes, polycyclic aromatic compounds, or heterocyclic compounds producing cyclic